Image guided surgery: clinical validation of lesion identification technologies and exploration of nerve sparing approaches

KleinJan, G.H.

Chapter 4

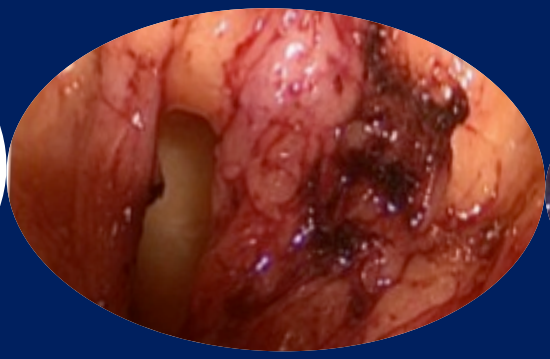

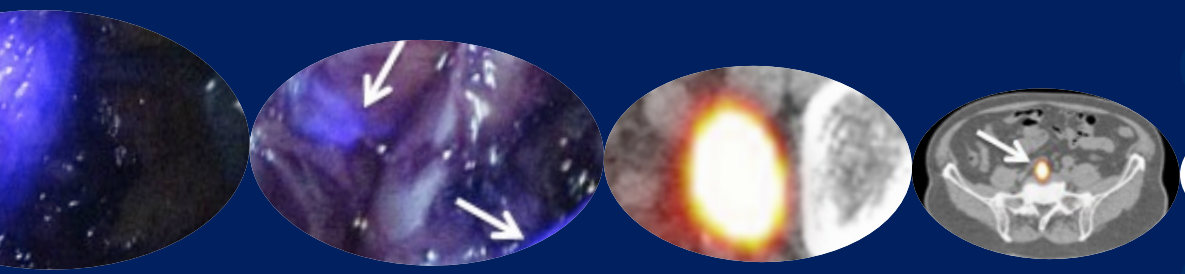

4

Optimization of fluorescence guidance during robot-assisted laparoscopic sentinel node biopsy for prostate cancer

*Gijs H. KleinJan**
*Nynke S. van den Berg**
Oscar R. Brouwer
Jeroen de Jong
Cenk Acar
Esther M. Wit
Eric Vegt
Vincent van der Noort
Renato A. Valdés Olmos
Fijs W.B. van Leeuwen
Henk G. van der Poel
Eur Urol. 2014;66:991-8.
** Authors share first authorship.*

ABSTRACT

INTRODUCTION

The hybrid tracer was introduced to complement intraoperative radiotracing towards the sentinel nodes (SNs) with fluorescence guidance. In this chapter the hybrid tracer preparation, injection technique, and fluorescence imaging hardware were adjusted to optimize the *in vivo* fluorescence-based SN identification for prostate cancer.

METHODS

Forty patients with a Briganti nomogram-based risk >5% of lymph node (LN) metastases were included. After intraprostatic tracer injection, SN mapping was performed (lymphoscintigraphy and single photon emission computed tomography with computed tomography (SPECT/CT)). In groups 1 and 2, SNs were pursued intraoperatively using a laparoscopic gamma probe followed by fluorescence imaging. In group 3, SNs were initially located via fluorescence imaging. Compared with group 1, in groups 2 and 3, a new tracer formulation was introduced that had a reduced total injected volume (2.0 mL vs. 3.2 mL but increased particle concentration. For groups 1 and 2, the Tricam SLII with D-Light C laparoscopic fluorescence imaging system was used. In group 3, the laparoscopic fluorescence imaging system was upgraded to an Image 1 HUB HD with D-Light P system. Number and location of the preoperatively identified SNs, *in vivo* fluorescence-based SN identification rate, tumor status of SNs and LNs, postoperative complications, and biochemical recurrence (BCR) were scored.

RESULTS

Mean fluorescence-based SN identification improved from 63.7% (group 1) to 85.2% and 93.5% for groups 2 and 3, respectively (p=0.012). No differences in postoperative complications were found. In three pN0 patients BCR occurred during follow up.

CONCLUSIONS

Stepwise optimization of the hybrid tracer formulation and the LFI system led to a significant improvement in fluorescence-assisted SN identification. Preoperative SPECT/CT remained essential for guiding intraoperative SN localization. Patient summary: Intraoperative fluorescence-based SN visualization can be improved by enhancing the hybrid tracer formulation and laparoscopic fluorescence imaging system.

INTRODUCTION

Sentinel node (SN) biopsy using a radioactive tracer was introduced for prostate cancer (PCa) to minimize the extent of the pelvic lymph node (LN) dissection (PLND) while retaining diagnostic accuracy [1]. The concept behind SN biopsy is to identify the LNs that are most likely to contain metastatic cells in case migration from the primary prostate tumor has occurred, the so-called SNs. Visualization of this direct drainage pathway transcends the anatomic location of the SN. Therefore, this technique also enables the identification of potential tumor-bearing LNs outside the extended PLND (ePLND) template [2,3] that would otherwise have been missed. When performing SN biopsy in combination with an ePLND, improved lymphatic staging can be achieved; pathologists can evaluate the SNs more extensively, decreasing the possibility of sampling errors, which can result in improved diagnostic accuracy [4,5].

Since its introduction, the procedure has been subject to various refinements. In the past 15 years, the surgical technique has shifted from a mainly open procedure to a laparoscopic and later a robot-assisted procedure. For preoperative SN mapping, following the injection of a radioactive tracer, lymphoscintigrams are taken. The introduction of single photon emission computed tomography with computed tomography (SPECT/CT) resulted in improved anatomic SN localization, allowing better planning of the operation and reducing operative time [6].

To date, intraoperative SN identification is based primarily on the use of a (laparoscopic) gamma probe (LGP; radio-guided approach). The recent introduction of fluorescence imaging (FI) during surgery was shown to aid the surgeon in optical, fluorescence-based, visualization of the SNs [7,8]. Yet, the limited penetration depth of the near-infrared fluorescent dye indocyanine green (ICG; < 1.0 cm) prohibits preoperative SN mapping, meaning that during surgery meticulous scanning of, and beyond, the entire ePLND template is required [2,6]. This exploration is extensive and time-consuming and may potentially miss SNs. Hence, the use of ICG is often combined with radiocolloid-based preoperative SN mapping methods [8]. To facilitate the integrated use of preoperative imaging with fluorescence guidance, we introduced the hybrid tracer ICG-^{99m}Tc-nanocolloid [6]. Being both radioactive and fluorescent, a single ICG-^{99m}Tc-nanocolloid administration allows for preoperative SN mapping as well as intraoperative fluorescence guidance to these exact hotspots. In our previous studies, the hybrid nature of this tracer was shown to complement the radio-guided approach and outperformed blue dye [9,10].
Following our initial feasibility study in PCa [11], 40 additional PCa patients were included. In

these patients, we systematically evaluated whether optimization of the tracer formulation and FI hardware improvements could help increase *in vivo* fluorescence-based SN identification during robot-assisted laparoscopic procedures.

METHODS

Patients

Between December 2010 and July 2013, 40 patients with localized PCa and a Briganti nomogram–estimated risk >10% of LN metastases were included after informed consent was obtained. Patients were scheduled for robot-assisted radical prostatectomy (RARP) and SN biopsy followed by an ePLND. The first nine patients were included under registration of the feasibility study (N09IGF), and the patient population was completed through off-label use of the hybrid tracer.

Three groups were formed for statistical analysis. In group 1 (n = 11; December 2010 – April 2011), the previously described hybrid tracer preparation [11] and the Tricam SLII with D-Light C laparoscopic fluorescence imaging (LFI) system (KARL STORZ GmbH & Co. KG, Tuttlingen, Germany) was used. In group 2 (n = 13; April 2011 – November 2012), the particle concentration was increased, and the injected volume decreased. In group 3 (n = 16; December 2012 – July 2013), the tracer formulation was identical to that used in group 2, but an upgraded LFI system (Image 1 HUB HD with D-Light P system KARL STORZ GmbH & Co. KG) was introduced.

Tracer preparation

Two different tracer formulations were used. In group 1, we prepared the hybrid tracer as previously described (0.4 ml in the syringe; referred to as the previously described tracer formulation) [11]. In groups 2 and 3, we used the new tracer formulation.

The new tracer formulation was prepared as follows: ^{99m}Tc-nanocolloid was made by adding 2.0 ml pertechnetate (approximately 300 MBq) to a vial of nanocolloid (GE Healthcare, Eindhoven, The Netherlands). ICG-^{99m}Tc-nanocolloid was then formed by adding 0.05 ml (0.25 mg) of ICG solution (5.0 mg/ml; PULSION Medical, Feldkirchen, Germany) to the vial. After in situ formation of ICG-^{99m}Tc-nanocolloid, the tracer was subtracted from the vial and diluted with saline to a total volume of 2.0 ml in the syringe. Procedures were performed in accordance with the Dutch guidelines for good manufacturing practice and with approval of the local pharmacist.

Tracer injection

The hybrid tracer was injected transrectally into the peripheral zone of each quadrant of the prostate under ultrasound guidance [11]. In group 1, four deposits of 0.1 ml ICG-^{99m}Tc-nanocolloid were given. After each injection, the needle was flushed with 0.7 ml saline (total injected volume: 3.2 ml). In groups 2 and 3, patients received four deposits of 0.5 ml ICG-^{99m}Tc-nanocolloid (total injected volume: 2.0 ml).

Preoperative sentinel node mapping

Static planar lymphoscintigraphy was performed 15 min and 2 h after injection, followed by a SPECT and low-dose CT scan (Symbia T; Siemens Healthcare, Erlangen, Germany). SPECT and low-dose CT images were fused, and a three-dimensional (3D) SPECT/CT–based volume-rendering reconstruction was created using OsiriX medical imaging software (Pixmeo, Geneva, Switzerland). Images were analyzed by an experienced nuclear medicine physician according to previously described criteria [12].

Surgical procedure

Operations were performed by HGvdP using the da Vinci S Surgical system (Intuitive Surgical Inc., Sunnyvale, CA, USA). Patients, first underwent SN biopsy, followed by ePLND and RARP. In the case of a one-sided SN non-visualization following preoperative imaging, an ePLND was performed on that side. The ePLND comprised all LNs in the internal, obturator, and external regions proximal of the ureter vessel crossing and distally from the pubic bone. SNs outside the ePLND template were defined as described by Meinhardt et al. [13].

Preoperatively acquired SPECT/CT images and the 3D volume-rendered image were used as a virtual roadmap for the localization of the individual SNs. Intraoperatively, in groups 1 and 2, SNs were initially pursued using an LGP (Europrobe 2; Eurorad, Eckbolsheim, France) followed by confirmatory FI. In group 3, SNs were initially localized via FI followed by *ex vivo* confirmation via gamma tracing. Real-time fluorescence images were introduced into the da Vinci S system via the TilePro function [11].

Fluorescence imaging hardware

In this study, two generations of laparoscopic fluorescence imaging systems were used: the Tricam SLII with D-Light C system (groups 1 and 2) and the Image 1 HUB HD with D-Light P system (group 3) (both KARL STORZ GmbH & Co. KG).

Pathologic examination

LNs and SNs were formalin fixed, cut at 2 mm, and paraffin embedded. LN sections were stained with haematoxylin and eosin (H&E). SNs were cut at three levels (150 nm intervals), and sections were H&E stained. In addition, on the second level, an immuno-histochemical stain was performed using a CAM5.2 antibody (catalogue number 345779; Becton Dickinson Biosciences, San Jose, CA, USA). Prostatectomy specimens were formalin fixed, paraffin embedded, and classified according to the 2009 TNM classification.

Follow-up

Postoperative complications (within 90 d post surgery) were scored using the Clavien-Dindo score [14]. Patients were evaluated for biochemical recurrence (BCR; prostate-specific antigen > 0.1 ng/ml) during follow-up.

Statistical analysis

For continuous variables, the mean or median and interquartile range (IQR; 25–75%) is given. For discrete variables, frequencies and percentages are reported. Study end points were as follows: intraoperative fluorescence-based SN identification rate - defined for each patient as ([number of SNs intraoperatively visualized via fluorescence imaging] / [total number of SNs seen on preoperative imaging]) x 100% -, postoperative complications, and BCR.

A one-way analysis of variance was performed for evaluation of the number of postoperative complications in the three groups. We used the nonparametric Kruskal-Wallis test for evaluation of between-group differences in intraoperative fluorescence-based SN identification rate and the number of harvested SNs and LNs. For BCR-free survival, we performed a log-rank test comparing groups 1 and 2 with group 3. A chi-square test was performed to evaluate whether there was a difference in pN1 patients among the three groups. Statistical analysis was performed using SPSS v.20 (IBM Corp., Armonk, NY, USA). In general, viewing our 40 patients as a random sample of the entire population, our null hypothesis is that the unknown distributions of these rates in the population are the same across the three groups. A p value <0.05 was considered significant.

	Total	Group 1	Group 2	Group 3
No. patients	40	11	13	16
Age, median (IQR)	64 (60-68)	62 (59-69)	64 (61-67)	65 (60-70)
Preoperative PSA-level (ng/mL), median (IQR)	8.5 (6.4-13.9)	12.0 (8.1-17.2)	9.0 (6.9-15.5)	6.8 (5.2-9.0)
Clinical T-stage				
- 1c (%)	7	2	3	2
- 2a (%)	3	1	1	1
- 2b (%)	10	4	3	4
- 2c (%)	9	1	3	4
- 3a (%)	9	3	2	4
- 3b (%)	2	0	1	1
Biopsy Gleason sum score				
- 6 (%)	4	4	0	0
- 7 (%)	30	6	8	16
- 8 (%)	5	1	4	0
- 9 (%)	1	0	1	0
- 10 (%)	0	0	0	0
Pathologic T-stage				
- 2a (%)	0	0	0	0
- 2b (%)	6	2	1	3
- 2c (%)	16	3	5	8
- 3a (%)	16	5	6	5
- 3b (%)	2	1	1	0
Pathologic Gleason sum score				
- 6 (%)	4	0	2	2
- 7 (%)	28	9	6	14
- 8 (%)	3	1	2	0
- 9 (%)	4	0	3	0
- 10 (%)	1	1	0	0

Table 1. Patient characteristics

IQR = interquartile range; no. = number; PSA = prostate specific antigen.

	Total (n=38[@])	Group 1	Group 2	Group 3	p-value
Number of intraoperatively detected SNs, per patient, median (IQR)	3 (2-4)	2 (2-3)	4 (2.5-4)	4 (2-4)	0.2[a]
In vivo SN identification					
- Fluorescence-based SN identification rate[#] in vivo, per patient, mean % (mean% corrected for malfunctioning equipment)	72.9% (84.0%*)	50.9% (63.7%*)	63.8% (85.2%*)	93.5% (93.5%*)	0.005[a] (0.012[a])
- Radioactivity-based SN detection in vivo, per patient, mean%	100%	100%	100%	NA	-
Ex vivo SN measurements					
- Fluorescence-based SN detection ex-vivo, %	96.9%	92.6%	97.7%	100.0%	-
- Radioactivity-based SN detection ex vivo, %	100.0%	100.0%	100.0%	100.0%	-
Time per combined SN, ePLND and prostatectomy procedure (h), median (IQR)	2:07 (2:00-2:12)	2:01 (1:50-2:01)	2:04 (2:00-2:14)	2:06 (2:02-2:14)	0.2[b]

Table 2. Intraoperative sentinel node identification and ex vivo measurements

[@] Two patients were excluded due to non-visualization on preoperative images (one patient in group 1, and one patient in group 2).

[#] Intraoperative fluorescence-based SN identification rate is defined as: defined for each patient as: ((number of SNs intraoperatively visualized via fluorescence imaging) / (total number of SNs seen on preoperative imaging)) x 100%.

* Intraoperative fluorescence-based SN identification rate after correction for non-visualization due to malfunctioning equipment.

[a] = Kruskal-Wallis test; [b] = ANOVA-test; n = number; NA = not applicable,

IQR = interquartile range; SN = sentinel node; n = number of patients.

RESULTS

Preoperative imaging

Patient characteristics are shown in Table 1. At least one SN was preoperatively identified in 38 of the 40 patients. Bilateral non-visualization occurred in two patients (5.0%) and unilateral non-visualization in five patients (12.5%). Lymphoscintigraphy and SPECT/CT identified a total of 119 SNs (median: 3; IQR: 0–2). Results per subgroup are specified in Supplemental Table 1. Changing the hybrid tracer formulation did not yield a significant difference in the number of preoperatively visualized SNs (Table 2). However, with the new tracer formulation, flushing was no longer necessary between placement of the different tracer deposits, thereby reducing injection time and increasing the ease of the procedure.

Intraoperative sentinel node identification

Six of the preoperatively identified SNs could not be resected because of the risk of injury or mechanical limitations of the robot (pararectal region inside the mesorectal fascia (n = 3), presacral region (n = 2), and right iliac region (n =1; Table 3).

In 7 patients, 14 additional SNs were removed during surgery based on their fluorescent and radioactive appearance in the same region as the SNs detected with preoperative imaging. In retrospect, in six of these seven patients, LN clusters could be visualized on CT (Figure 1). Overall, 127 SNs (median: 3 per patient; IQR: 2–4; Table 2) were identified during surgery. In 16 patients (40.0%), an SN was located outside the ePLND template (Figs. 2 and 3; Table 3). The two patients who had non-visualization on preoperative imaging were excluded from the intraoperative SN detection outcome analysis. With every stepwise modification, the intraoperative fluorescence-based SN visualization rate increased (Table 2). The mean optical SN visualization percentage modestly increased from 50.9% (group 1) to 63.8% (group 2) after the tracer formulation was altered. In these two groups, in five patients (group 1: two patients; group 2: three patients), none of the SNs could be intraoperatively visualized via FI for reasons of malfunctioning equipment (damaged light cable). After excluding these patients, the in vivo fluorescence-based SN visualization percentage of groups 1 and 2 was found to be 63.7% and 85.2%, respectively. Following the introduction of the upgraded LFI system (group 3), the mean intraoperative visualization percentage went up to 93.5% (p = 0.012). *Ex vivo* measurements in the operating room revealed a fluorescent signal in 123 of the 127 excised SNs.

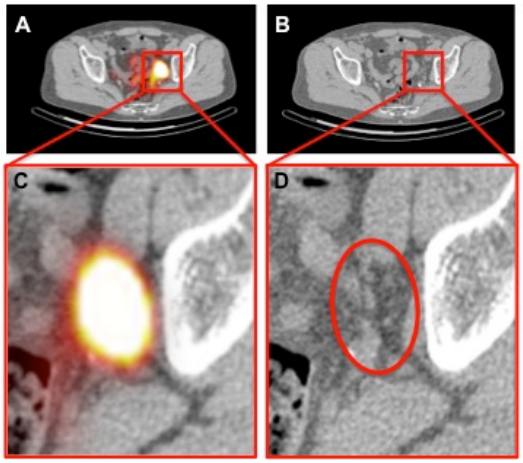

Figure. 1. Clustered lymph nodes as seen on single-photon emission computed tomography with computed tomography (SPECT/CT) imaging:

(A) Fused SPECT/CT image showing the location of a single radioactive hotspot in the left obturator region;

(B) corresponding CT image; **(C)** zoom showing the radioactive hotspot; **(D)** multiple lymph nodes were visualized on the CT image in the area of the radioactive hotspot.

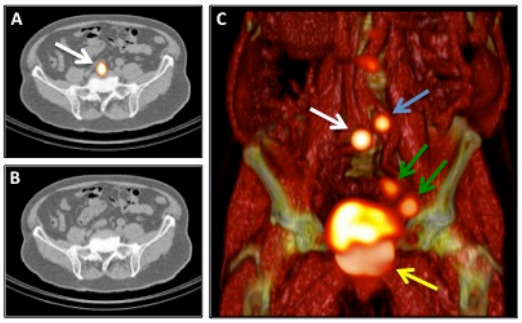

Figure 2. Illustration of the localization of sentinel nodes (SNs) outside the extended pelvic lymph node dissection template:

(A) Fused single-photon emission computed tomography with computed tomography (CT) image showing the location of a single radioactive hotspot at the aorto-caval level (white arrow);

(B) corresponding CT image;

(C) three-dimensional volume rendering showing the injection site (yellow arrow), the aorto-caval SN (white arrow), and two SNs at the external iliac and obturator region (green arrows). A higher-echelon para-aortic lymph node (blue arrow) was also visualized.

Pathologic examination

Overall, histopathologic analysis of the excised tissues yielded 467 LNs: 160 nodes in the SN specimens and 307 additional nodes resected from the subsequent ePLND template. In 8 patients, a total of 32 tumor-positive nodes was found: 16 SNs and 16 LNs (Table 4; Supplemental Table 2). In three patients, the SN was the only tumor-positive node. In three other patients, next to a tumor-positive SN, a tumor-positive LN was also found. Strikingly, in 1 of these 3 patients, next to 2 tumor-positive SNs, we found 12 tumor-positive LNs (Supplemental Table 2). In the last two positive patients, SNs were tumor free, but a tumor-positive LN was found. In one of these two patients, the positive LN was found in the ePLND tissue (false-negative SN biopsy procedure). In the other patient, a small positive LN (3 mm) was found in the prostatectomy specimen. This particular LN was not seen on preoperative images.

On a per-patient basis, the sensitivity of the SN biopsy procedure was 75.0% (six out of eight pN1 patients correctly staged with SN biopsy), with a negative predictive value of 94.1%. On a per–tumor-positive node basis, this sensitivity is 50.0% (16 tumor-positive SNs on a total of 32 positive nodes; Table 4).

3.4. Follow-up

No significant differences in postoperative complications were found among the three groups (p = 0.9; Table 5). Although follow-up was relatively short, in patients without nodal metastases (pN0), the Kaplan-Meier curve showed an improvement in BCR-free survival in group 3 (n = 0; total follow-up: 25 months) versus men in groups 1 and 2 (n = 3; total follow-up: 38 months; p = 0.2; Figure 4).

Discussion

This study demonstrates that optimization of the hybrid tracer formulation and injection technique, as well as upgrading the LFI system, improved *in vivo* fluorescence-based SN identification during RARP. Without altering the efficacy of preoperative SN mapping, the new tracer formulation increased the injected amount of ICG-^{99m}Tc-nanocolloid particles 2.5-fold and reduced the injected volume 1.6-fold. In combination with initial LGP exploration, the *in vivo* fluorescence visualization efficiency increased by 21.5% (group 1 vs. group 2). This increase contradicts our previous findings in breast cancer patients, where a 2-fold increase in the amount of injected particles did not lead to a change in fluorescence visualization efficiency [15]. Feedback from previous studies taught us that the SN has to be exposed within millimeters of the surface to allow for *in vivo* fluorescence-based detection

	Total	Group 1	Group 2	Group 3
SNs removed from ePLND template, no. (% total)				
- Left obturator region	19 (15.0%)	4 (3.1%)	4 (3.1%)	11 (8.7%)
- Right obturator region	28 (22.0%)	7 (5.5%)	10 (7.9%)	11 (8.7%)
- Left external region	18 (14.2%)	6 (4.7%)	8 (6.3%)	4 (3.1%)
- Right external region	16 (12.6%)	5 (3.9%)	5 (3.9%)	6 (4.7%)
- Left internal region	9 (7.1%)	0	5 (3.9%)	4 (3.1%)
- Right internal region	7 (5.5%)	0	2 (1.6%)	5 (3.9%)
- Left common Iliac trunk	10 (7.9%)	3 (2.4%)	4 (3.1%)	3 (2.4%)
- Right common Iliac trunk	2 (1.6%)	0	0	2 (1.6%)
Subtotal	109 (85.8%)	25 (19.7%)	38 (29.9%)	46 (36.2%)
SN removed outside ePLND template, no. (% total)				
- Pararectal (mesorectal fascia) region	5 (3.9%)	1 (0.8%)	0	4 (3.1%)
- Presacral region	5 (3.9%)	1 (0.8%)	2 (1.6%)	2 (1.6%)
- Paravesical region	4 (3.1%)	0	0	4 (3.1%)
- Right umbilical ligament	1 (0.8%)	0	1 (0.8%)	0
- Left umbilical ligament	1 (0.8%)	0	1 (0.8%)	0
- Para-aortal region	2 (1.6%)	0	2 (1.6%)	0
Subtotal	18 (14.2%)	2 (1.6%)	6 (4.7%)	10 (7.9%)
Total	127 (100.0%)	27 (21.3%)	44 (34.6%)	56 (44.1%)
Not removed SN, no.				
- Pararectal region	3	1	1	1
- Presacral region	2	0	1	1
- Right iliac region	1	1	0	0
Total	6	2	2	2

Table 3. Number and location of the intraoperatively identified sentinel nodes

SN = sentinel node; ePLND = extended pelvic lymph node dissection; no. = number.

	Total	Group 1	Group 2	Group 3	p-value
No. patients pN1	8	2	3	3	0.9[b]
SN evaluation					
- No. harvested SNs / patient, median (IQR)	4 (2.3-5.0)	3 (2.0-3.0)	4 (2.5-5.5)	4 (3.0-5.8)	0.028[a]
- Total no. SNs	160	29	57	74	
- Total no. tumor-positive SNs	16	1	5	9	
LN evaluation					
- No. harvested LNs from ePLND/patient, median (range)	8 (4.5-11.0)	4 (4.0-10.0)	6 (4.5-12.0)	9 (7.3-11.0)	0.2[a]
- Total no. LNs	307	65	95	147	
- Total no. tumor-positive LN	16	1	13	2	
SN + LN evaluation					
- Total no. removed nodes per patient (SN + ePLND), median (IQR)	12 (9.0-14.8)	9 (6.0-11.0)	11 (8.0-15.5)	12 (11.0-16.0)	0.026[a]
- Total no. harvested SNs + LNs	467	94	152	221	

Table 4. Pathologic node evaluation

[a] = Kruskal-Wallis test; [b] = Chi-square test.

no. = number of patients; IQR = interquartile range; No. = number; SN = sentinel node; LN = lymph node; ePLND = extended pelvic lymph node dissection; pN1 = positive for regional lymph node metastases.

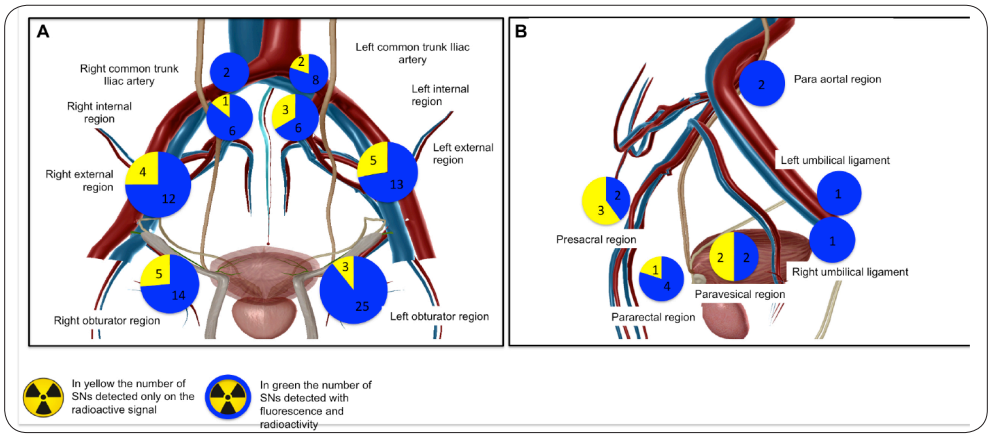

Figure 3. Intraoperative sentinel node (SN) location.

(A) SNs inside the extended pelvic lymph node dissection (ePLND) template;

(B) SNs outside the ePLND template. Intraoperatively, nodes were detected using radio-guidance (yellow) or radio-and fluorescence guidance (blue). The schematic images used to illustrate the location of the detected SNs were generated with Visible Body software (Argosy Publishing, Newton Upper Falls, MA, USA).

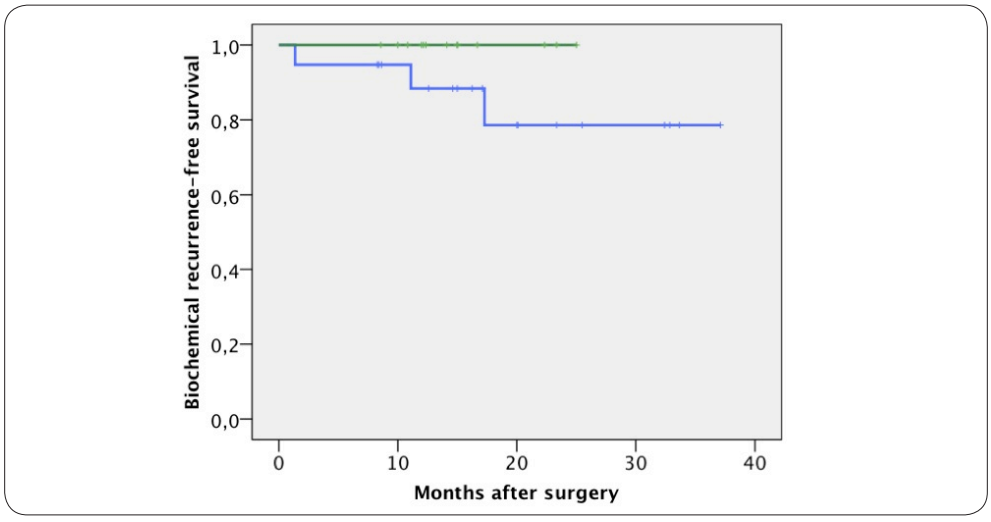

Figure 4. Kaplan-Meier curve illustrating biochemical recurrence (BCR) in pN0 patients.

The blue line represents groups 1 and 2, in which three BCRs were found. The orange line represents group 3.

[9,10,16]. Hence, an explanation for this finding may lie in the time taken for the now more routine surgical exploration; findings in group 1 turned out lower than the reported 85% in our feasibility study, which was based on the same approach.
After upgrading the LFI system (group 3), the mean intraoperative fluorescence-based SN visualization percentage increased to 93.5%, transforming the procedure in a potential driver to improve intraoperative localization of tumor-positive SNs, even within the standard ePLND template. This improvement may provide better nodal staging (the "Will Rogers" phenomenon) and help improve the BCR-free survival rate, as was seen in group 3 [17]. The tailored filter settings allowed visualization of the near-infrared fluorescence signal (displayed in blue) as an integral part of the patient anatomy (displayed in "normal" colored view; Figure 5). Despite a slight loss in sensitivity, this continuous exploration of the surgical field via FI proved extremely valuable for the localization of the SN. In combination with the 3D information that SPECT/CT provided, this improvement may render initial exploration with the LGP *in vivo* redundant, provided that the fluorescence-based SN identification rate equals that of its radioactive counterpart. This is attractive because fluorescence does not suffer from the shine-through phenomenon from the tracer deposits in the prostate, as is the case for the radio-guided approach [18].

Of the 16 tumor-positive SNs that were resected during the operation, one was located outside the ePLND template (6.3%). This finding underlines previous reports stating that metastatic spread may occur beyond the ePLND template [13,19]. In 5 of the 8 LN-positive patients, we found positive LNs beyond the resected SNs; in total, 16 additional tumor-positive LNs were recovered from the ePLND specimens. It must be noted that one patient accounts for 75% of these positive LNs (Supplemental Table 2). Based on our findings, we believe that SN identification via the hybrid approach (including SPECT/CT) combined with ePLND provides the best approach for nodal staging in combination with RARP.
The main limitations of the study are the small patient population, the possibility that SN identification rates may increase over time because of a learning curve, and the relatively low number of overall nodes removed. The cost-effectiveness and the independent use of intraoperative fluorescence guidance remain to be investigated; currently, an international multicenter study is being initiated to address this question. Still an important question remains to be answered: What is the best hybrid tracer injection technique? In our current, ongoing study (N12IGP), we will evaluate whether the location of hybrid tracer injection (intraprostatic vs. intratumoural) is relevant for the detection and localization of tumor-positive SNs.

	Total	Group 1	Group 2	Group 3
No. patients	40	11	13	16
Injected dose (MBq), median (IQR)	217.8 (205.3-228.7)	218.2 (205.7-236.7)	223.8 (207.8-236.7)	209.6 (203.8-222.8)
Preoperative imaging results, no. per patient				
- SNs on early lymphoscintigrams, median (IQR)	1 (0-2)	1 (0-2)	1 (0-2)	1 (0-2)
- SNs on late lymphoscintigrams, median (IQR)	2 (1-3)	2 (2-3)	2 (1-3)	2 (2-3)
- SNs on SPECT/CT, median (IQR)	3 (0-6)	2 (2-3)	4 (2-4)	3 (2-4)
- Higher-echelon LNs, median (IQR)	0 (0-1)	1 (0-2)	0 (0-1)	0 (0-.75)
Time from injection to surgery (h), median (IQR)	5:44 (4.15-5.07)	4:34 (4:15-5:05)	5:05 (4:14-5:35)	4:42 (4:13-5:04)

Table SI-1. Preoperative imaging results

MBq = Mega Bequerel; IQR = interquartile range; SN = sentinel node;LN = lymph node; n = number of patients; no. = number; SPECT/CT = single photon emission computed tomography combined with computed tomography.

Patient	No. tumor-positive SNs	Location tumor-positive SNs	No. tumor-positive LNs from ePLND	Total no. tumor-positive SNs + LNs from ePLND
1	0/1	-	1/3	1/4
2	1/7	Right external region	0/4	1/13
3	1/12	Right external region	1/7	2/19
4	2/2	Left internal region, Right obturator region	12/13	14/15
5	3/3	Left external region (2x), Left paravesical region	0/8	3/11
6	0/3	-	1/12	1/15
7	5/9	Left internal region (4x), Right obturator region	0/12	5/21
8	4/6	Left external region, Left obturator region, Right internal region, Right obturator region	1/13	5/19
Total	16/43		16/72	32/115

Table SI-2. pN1 Pathological findings

SN = sentinel node; LN = lymph node; ePLND = extended pelvic lymph node dissection.

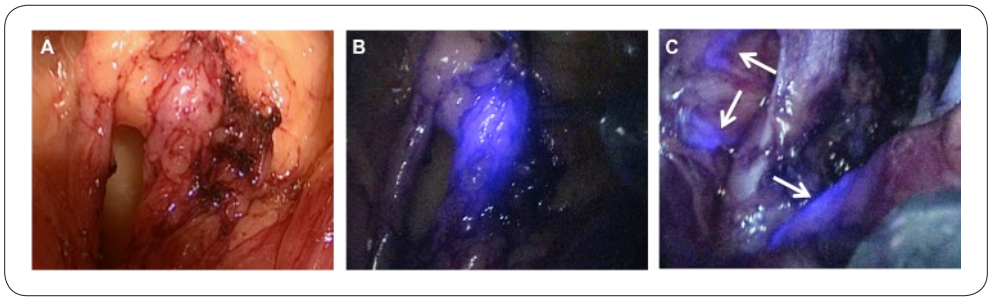

Figure 5. Intraoperative sentinel node (SN) and lymphatic duct identification via fluorescence guidance:

(A) white-light image illustrating the area that harbors the SN;

(B) fluorescence guidance clearly shows the contours of the SNs (the adjusted filter settings of the Image 1 HUB HD with D-Light P system (KARL STORZ GmbH & Co. KG, Tuttlingen, Germany) allows clear visualization of anatomic detail in the background);

(C) lymphatic ducts visualized via fluorescence imaging (white arrows).

CONCLUSION

Altering the hybrid tracer formulation and injection technique and upgrading the LFI system significantly improved *in vivo* fluorescence-based SN identification. Further improvement of *in vivo* fluorescence-based SN detection, reaching rates similar to that of the conventional radio-guided approach, may make intraoperative LGP redundant. Still, SPECT/CT remains an essential tool for preoperative SN localization.

REFERENCES

1. Wawroschek F, Vogt H, Weckermann D, Wagner T, Harzmann R. The sentinel lymph node concept in prostate cancer - first results of gamma probe-guided sentinel lymph node identification. Eur Urol 1999;36:595–600.
2. Van Leeuwen FWB, Hruby S. Fluorescence guidance during radical prostatectomy. Eur Urol 2014;65:1169–1170.
3. Rousseau C, Rousseau T, Campion L, et al. Laparoscopic sentinel lymph node versus hyperextensive pelvic dissection for staging clinically localized prostate carcinoma: a prospective study of 200 patients. J Nucl Med 2014;55:753–758.
4. Staník M, Capák I, Macík D, et al. Sentinel lymph node dissection combined with meticulous histology increases the detection rate of nodal metastases in prostate cancer. Int Urol Nephrol. In press. http://dx.doi.org/10.1007/s11255-014-0704-3
5. Wawroschek F, Wagner T, Hamm M, Weckermann D, Vogt H, Ma B. The influence of serial sections, immunohistochemistry, and extension of pelvic lymph node dissection on the lymph node status in clinically localized prostate cancer. Eur Urol 2003;43:132–137.
6. Warncke SH, Mattei A, Fuechsel FG, Brun SZ, Krause T, Studer UE. Detection rate and operating time required for probe-guided sentinel lymph node resection after injection of technetium-^{99m} nanocolloid into the prostate with and without preoperative imaging. Eur Urol 2007;52:126–133.
7. Manny TB, Patel M, Hemal AK. Fluorescence-enhanced robotic radical prostatectomy using real-time lymphangiography and tissue marking with percutaneous injection of unconjugated indocyanine green: the initial clinical experience in 50 patients. Eur Urol 2014;65:1162–1168.
8. Jeschke S, Lusuardi L, Myatt A, Hruby S, Pirich C, Janetschek G. Visualization of the lymph node pathway in real time by laparoscopic radioisotope-and fluorescence-guided sentinel lymph node dissection in prostate cancer staging. Urology 2012;80:1080–1087.
9. Brouwer OR, van den Berg NS, Mathe´ron HM, et al. A hybrid radioactive and fluorescent tracer for sentinel node biopsy in penile carcinoma as a potential replacement for blue dye. Eur Urol 2014;65:600–609.
10. Matheron HM, van den Berg NS, Brouwer OR, et al. Multimodal surgical guidance towards the sentinel node in vulvar cancer. Gynecol Oncol 2013;131:720–725.
11. Van der Poel HG, Buckle T, Brouwer OR, Valde´s Olmos RA, van Leeuwen FWB. Intraoperative laparoscopic fluorescence guidance to the sentinel lymph node in prostate cancer patients: clinical proof of concept of an integrated functional imaging approach using a multimodal tracer. Eur Urol 2011;60:826–33.
12. Nieweg OE, Tanis PJ, Kroon BB. The definition of a sentinel node. Ann Surg Oncol 2001;8:538–541.
13. Meinhardt W, van der Poel HG, Valde´s Olmos RA, Bex A, Brouwer OR, Horenblas S. Laparoscopic sentinel lymph node biopsy for prostate cancer: the relevance of locations outside the extended dissection area. Prostate Cancer 2012:751753.
14. Dindo D, Demartines N, Clavien P-A. Classification of surgical complications: a new proposal with evaluation in a cohort of 6336 patients and results of a survey. Ann Surg 2004;240:205–213.
15. Schaafsma BE, Verbeek FPR, Rietbergen DDD, et al. Clinical trial of combined radio-and fluorescence-guided sentinel lymph node biopsy in breast cancer. Br J Surg 2013;100:1037–1044.
16. Brouwer OR, Klop WMC, Buckle T, et al. Feasibility of sentinel node biopsy in head and neck melanoma using a hybrid radioactive and fluorescent tracer. Ann Surg Oncol 2012;19:1988–1994.
17. Gofrit ON, Zorn KC, Steinberg GD, Zagaja GP, Shalhav AL. The Will Rogers phenomenon in urological oncology. J Urol 2008;179:28–33.
18. Fukuda M, Egawa M, Imao T, Takashima H, Yokoyama K, Namiki M. Detection of sentinel node micrometastasis by step section and immunohistochemistry in patients with prostate cancer. J Urol 2007;177:1313–1317.
19. Joniau S, Van den Bergh L, Lerut E, et al. Mapping of pelvic lymph node metastases in prostate cancer. Eur Urol 2013;63:450–458.